PRIFYSGOL ABERYSTWYTH UNIVERSITY

Aberystwyth University

Hydrogen Production from Coke Oven Gas by CO2 Reforming Over a Novel Ni-Doped Silicalite-1

Wang, Dan; Wang, Jingfeng; Lu, Changyuan; Zou, Xingli; Cheng, Hongwei; Ning, Jinyan; Lu, Xionggang; Zhou, Zhongfu

Published in:
Catalysis Letters

DOI:
10.1007/s10562-018-2297-4

Publication date:
2018

Citation for published version (APA):
Wang, D., Wang, J., Lu, C., Zou, X., Cheng, H., Ning, J., Lu, X., & Zhou, Z. (2018). Hydrogen Production from Coke Oven Gas by CO2 Reforming Over a Novel Ni-Doped Silicalite-1. *Catalysis Letters*, *148*(5), 1424-1434. https://doi.org/10.1007/s10562-018-2297-4

General rights
Copyright and moral rights for the publications made accessible in the Aberystwyth Research Portal (the Institutional Repository) are retained by the authors and/or other copyright owners and it is a condition of accessing publications that users recognise and abide by the legal requirements associated with these rights.

• Users may download and print one copy of any publication from the Aberystwyth Research Portal for the purpose of private study or research.
• You may not further distribute the material or use it for any profit-making activity or commercial gain
• You may freely distribute the URL identifying the publication in the Aberystwyth Research Portal

Take down policy
If you believe that this document breaches copyright please contact us providing details, and we will remove access to the work immediately and investigate your claim.

tel: +44 1970 62 2400
email: is@aber.ac.uk

Download date: 04. May. 2023

Hydrogen Production from Coke Oven Gas by CO_2 Reforming Over a Novel Ni-Doped Silicalite-1

Dan Wang, [1]

Jingfeng Wang, [2]✉

Email jingfeng1101@126.com

Changyuan Lu, [1]

Xingli Zou, [1]

Hongwei Cheng, [1]

Jinyan Ning, [1]

Xionggang Lu, [1]

Zhongfu Zhou, [1]✉,[3]

Email z.zhou@shu.edu.cn

[1] State Key Laboratory of Advanced Special Steel & School of Materials Science and Engineering, Shanghai University, 99 Shangda Road, Shanghai, 200444 China

[2] National Engineering Research Center for Nanotechnology, 28 East Jiangchuan Road, Shanghai, 200241 China

[3] Department of Physics, Aberystwyth University, Aberystwyth, SY23 3BZ UK

Received: 20 September 2017 / Accepted: 4 January 2018

Abstract

A series of in-situ nickel atoms doped (Ni-doped) Silicalite-1 used as the catalysts in dry reforming of coke oven gas (COG) have been synthesized by one-pot hydrothermal method. These catalyst materials are characterized by electron microscopy, X-ray powder diffraction, and Nitrogen adsorption–

desorption measurements, etc. And the catalytic results show that in-situ Ni-doped zeolites exhibit superior performance for dry reforming of COG. Moreover, the in-situ synthesized Ni-doped Silicalite-1 catalysts with trace amount of nickel behave quite considerable activity and outstanding anti-coking property in comparison with the traditional Ni-based catalysts. The method we adopt in this work is less complicated for the synthesis of Ni-doped Silicalite-1, which will make the in-situ Ni-doped Silicalite-1 catalysts have great prospects for hydrogen production from COG by CO_2 reforming in the future.

Graphical Abstract

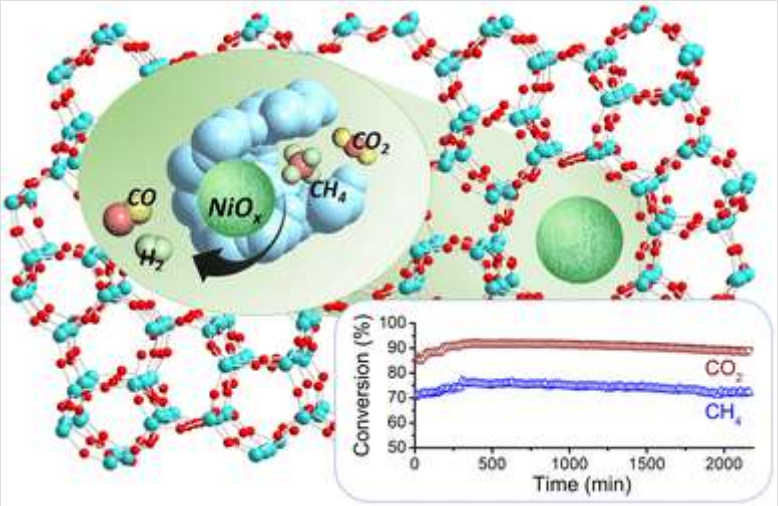

Keywords

In-situ Ni-doped Silicalite-1
One-pot hydrothermal method
Hydrogen production
Coke oven gas (COG)

1. Introduction

Regarded as the most promising alternative energy source, hydrogen has attracted worldwide attention owing to its highly efficiency, environmental friendliness and abundant sources characters [1, 2]. H_2, along with CH_4, CO and CO_2, is the primary component of syngas, which is mainly generated by CO_2 reforming of coke oven gas (COG) [3, 4]. Dry reforming of COG is thought to be an environmental friendly approach attracting particular interest as it generates clean energy from greenhouse effect gases [5, 6]. Lots of studies have

focused on developing highly efficient and stable catalysts for CO_2 reforming of CH_4 in the past decades [3, 5, 6, 7, 8]. For example, noble metals (Pt, Rh, Ru, etc.) particles [9] supported on Al_2O_3 [10], La_2O_3 [11], ZrO_2 [12], Y_2O_3–ZrO_2 [13] and other binary oxides [14, 15] as the catalysts have been designed in recent years. However, most of these noble metal catalysts are expensive, which has restricted availability in this reaction. Therefore, some alternative active metals, such as metal nickel, have been selected and developed for application in COG [16].

AQ1

Despite of great progress in hydrogen production from COG catalyzed by the Ni-based catalysts, there are still some drawbacks to be unsolved. Great attention has been paid to the catalyst deactivation caused by coke deposition [17, 18], which block the active sites on the surface of catalyst, preventing the reactant gases from getting access. Until now, it is envisaged to find an effective support to enhance the anti-coking property and improve the catalytic activity of Ni-based catalysts.

AQ2

Zeolites are potential catalyst supports with great promise because of their ultrahigh surface area, which provide countless active sites during the reaction [19, 20, 21, 22]. Besides, most of advantages, such as low density and high temperature stability [23, 24, 25], have brightened their application prospect. Nowadays, nickel ions modified zeolites for dry reforming of COG or CH_4 have attracted much attention for their reduced coke deposition [26, 27, 28]. It is highly desirable to design a novel zeolite catalyst for hydrogen production in COG.

In this paper, we report the synthesis of a series of Ni-doped Silicalite-1 catalysts with the remarkable catalytic activity and anti-coking ability via in-situ hydrothermal method. It is found that most nickel atoms can disperse uniformly not only on the material's surface, but also in the pores and channels of crystals. The catalytic efficiency of the in-situ Ni-doped Silicalite-1 and the influence of nickel contents on the catalytic activity in the CO_2 reforming of COG have been discussed in this paper. High catalyst activity and low coke deposition amount are acquired for the obtained in-situ Ni-doped Silicalite-1 materials due to the reactant gases act adequately in the channels and pores of the crystals. Meanwhile, we find that in-situ Ni-doped Silicalite-1 catalysts with even trace amount of doped nickel show desired catalytic activity, while Ni^{2+}-dipped Silicalite-1 obtained by traditional solution impregnation method has little activity in the CO_2 reforming of COG.

2. Experimental

2.1. Preparation of Catalysts

2.1.1. Preparation of Pure Silicalite-1

Silicalite-1 was obtained by a static hydrothermal method as described previously [29]. Firstly, the white Silicalite-1 gel precursor was prepared. $Si(OEt)_4$ (Et = ethyl), NEt_3, $[CH_3(CH_2)_2]_4NBr$ (TPABr) and H_2O with the molar ratio of $n(Si(OEt)_4):n(TPABr):n(NEt_3):n(H_2O) = 1:0.2:0.5:40$ were stirred for 1 h at room temperature, generating a clear Silicalite-1 aqueous solution. This Silicalite-1 solution was then transferred into a round flask and heated at 70 °C in vacuum for 1.5 h to remove the solvents such as H_2O, NEt_3, and EtOH. Subsequently, white gelatinous masses were prepared. The precursor gel was mixed with an aqueous solution of NEt_3 in a molar ratio of $n(SiO_2):n(NEt_3):n(H_2O) = 1:3:40$. After stirring for 2 h, the suspension was transferred into a Teflon-lined stainless vessel and heated at 170 °C for 7 days. The white samples were then filtered, washed with deionized water, and dried at 80 °C for 24 h. Finally, samples were calcined at 800 °C for 3 h with a ramp rate of 4 °C/min.

2.1.2. Preparation of In-Situ Ni-Doped Silicalite-1

Ni-doped Silicalite-1 catalysts were synthetized by in-situ hydrothermal method. Firstly, the white Silicalite-1 gel was also prepared. This TPABr-containing silica gel was then mixed with an aqueous solution of NEt_3 and $NiCl_2 \cdot 6H_2O$with different molar ratios listed in Table 1. After stirring for 2 h, the suspensions were then transferred into a Teflon-lined stainless vessel and preserved at 170 ~ 200 °C for 7 ~ 10 days. Subsequently, the synthesized samples were filtered and washed. Finally, after drying, the Ni-doped Silicalite-1 was obtained after calcination at 800 °C for 3 h with a ramp rate of 4 ° C/min There seems to be something wrong with the font of "o" in "°C". The unit should be "°C/min". .

Table 1

The molar ratio of raw materials in the synthesis process of pure Silicalite-1 and Ni-doped Silicalite-1 samples

Chemical component	SiO_2	Ni^{2+}	TPABr	NEt_3	H_2O	Samples synthesized
Molar ratio	1	0	0.18	3	40	Silicalite-1
		0.001				NS-001
		0.002				NS-002

Chemical component	SiO	Ni	TPABr	NEt	H O	Samples synthesized
		0.003				NS-003

As shown in Table 1, the pure Silicalite-1 containing no nickel is marked as Silicalite-1, and in-situ obtained Ni-doped samples with the silicon/nickel atom molar ratio of 1000/1, 1000/2, 1000/3, respectively, are marked as NS-001, NS-002, NS-003, respectively.

2.1.3. Preparation of Ion-Dipped Ni^{2+}-Silicalite-1

For comparison, an ion-dipped Ni^{2+}-Silicalite-1 was prepared by introducing Ni^{2+} cations into the zeolite crystals via solution impregnation. The impregnation reaction was conducted by treating Silicalite-1 zeolite with the aqueous solution of $NiCl_2 \cdot 6H_2O$ with the mole ratio n(Si):n(Ni) = 1000:1, the same as that of NS-001 zeolite. After stirring for 24 h, the ion-dipped Silicalite-1 was filtered, and dried in an oven at 80 °C for 24 h. Ion-dipped Ni^{2+}-Silicalite-1 is marked as Ni-S-1.

2.2. Characterization

The crystalline structure of Ni-doped Silicalite-1 materials was determined by X-ray powder diffraction (XRD) measurement (Rigaku D/MAX-2500, Japan) conducted with Cu Kα radiation.

The elements content was measured by inductively coupled plasma (ICP-OES) (PerkinElmer 7300DV, Waltham, MA, America).

X-ray photoelectron spectroscopy (XPS, ESCALAB 250 Xi, America) using Al Kα radiation with energy of 1486.6 eV was employed to obtain the chemical states of elements and bonding in the catalysts.

The morphology of zeolites was observed by scanning electron microscope (SEM, JSM-6700F, JEOL Ltd., Japan) at an acceleration voltage of 15 kV. The microstructure of the crystallites was characterized by transmission electron microscopy (TEM, JEM-2010F, JEOL Ltd., Japan), operating at 200 kV.

Thermogravimetric analysis and differential scanning calorimetry (TG-DSC, STA 449 F3, Netzsch) measurements were conducted to detect thermostability and carbon deposition of the catalysts before and after the catalytic reaction. The experiment was carried out by heating from room temperature to 1000 °C at a ramp rate of 10 °C/min in 10 mol% O_2/N_2 mixture (50 mL/min).

Nitrogen adsorption–desorption measurements were carried out using a Micromeritics ASAP 2020 physisorption analyzer. The Brunauere–Emmette–Teller (BET) surface area and pore structure of the Ni-doped Silicalite-1 samples after calcination were determined at − 196 It should be "-196" (minus 196). °C. Before the measurements, more than 100 mg of the catalyst was degassed under N_2 atmosphere at 250 °C for at least 6 h.

Temperature-programmed reduction (TPR) was conducted on Micrometrics AutoChem II 2920 instrument. Prior to the measurement, 0.1 g sample was pretreated under Ar flow (30 mL/min) at 200 °C for 0.5 h to remove moisture and other absorbed impurities, and then cooled to 100 °C. The temperature was raised to 900 °C at the ramp rate of 10 °C/min with a gas mixture of 10 mol% H_2/Ar (30 mL/min). The amount of H_2 uptake was measured with a thermal conductivity detector (TCD). In the reduction, an isopropanol trap was used to remove the generated water.

Temperature-programmed oxidation (TPO, Micrometrics AutoChem II 2920, America) was conducted to determine the amount of carbonaceous deposition under reaction conditions. During the reactive process, TPO was conducted in a micro-reactor coupled to a quadrupole mass spectrometer. About 50 mg sample was purged in Ar atmosphere at 200 °C for 30 min to remove the superficial moisture and adsorbed impurities, and then cooled down to 80 °C. After this pretreatment, the sample was heated in 10 mol% O_2/He mixture (30 mL/min) at the ramp rate of 10 °C/min up to 850 °C and remained 10 min.

2.3. Catalytic Activity Measurements

Catalytic experiments for dry reforming of COG were carried out in a fixed-bed quartz reactor with the inner diameter of 6 mm. Before the reaction, 0.2 g catalyst was treated in a mixture gas of 15 mol% H_2/N_2 for 12 h at 800 °C. Then the catalytic experiment was carried out at 800 °C by controlling the CH_4/CO_2 ratio which was under the stoichiometric condition for the dry reforming of methane and the total feed gas (also known as model COG, a mixture of pure gases: 24.35 mol% CH_4, 24.35 mol% CO_2, 5.64 mol% CO and 45.66 mol% H_2) flow rate of 100 mL/min under atmospheric pressure. The gas flow rate was controlled through mass flow controller. The resultants were dehydrated by the purifier and then analyzed by an online gas chromatograph equipped with a TCD. The flow rate of outlet gas was measured by a soap-membrane flowmeter. And the composition of the outlet gas was analyzed by external standard method. The conversions and selectivities were calculated as follows:

1

$$X_{CH_4} = \frac{F_{CH_4} - F_{CH_4}}{F_{CH_4,in}} \times 100\%$$

$$X_{CO_2} = \frac{F_{CO_2} - F_{CO_2}}{F_{CO_2,in}} \times 100\% \quad (2)$$

$$S_{H_2} = \frac{F_{H_2,out}}{F_{H_2,in} + 2\left(F_{CH_4,in} - F_{CH_4,out}\right)} \times 100\% \quad (3)$$

$$S_{CO} = \frac{F_{CO,out}}{F_{CO,in} + \left(F_{CH_4,in} - F_{CH_4,out}\right) + \left(F_{CO_2,in} - F_{CO_2,out}\right)} \times 100\% \quad (4)$$

3. Results and Discussion

XRD patterns of different samples are shown in Fig. 1. The as-made Siliciliate-1 sample presents well-resolved reflections, revealing the formation of MFI framework structure. For the samples of NS-001, NS-002, NS-003 and Ni-S-1, several well-resolved reflections to the structural configuration of zeolite Silicilate-1 are clearly observed. Besides, no diffraction peaks for impurity phases appear, suggesting no bulky or gathered particles of nickel or any form of nickel oxides (NO_x) exist in the samples. Furthermore, the XRD patterns of Ni-doped samples show a slightly shift compared with that of Silicalite-1 zeolite (see the inserted window). Assuming that there are 24 Si atoms per unit cell, there is theoretically 0.2–0.9 Ni atom (calculated according to the elemental composition measured by ICP, Table 2) in each unit cell of Ni-doped crystals, which could cause a slight lattice distortion in the crystal structure corresponding to the diffraction shift. Therefore, we conclude that most of the in-situ introduced nickel disperse uniformly in the pores or channels of crystals in some form of nickel species. XRD analysis also indicates that the crystallinity of the in-situ Ni-doped samples is slightly decreased with the amounts of nickel increase. Obviously, the introduction of nickel into the zeolite can decrease the crystallinity of crystals.

Fig. 1

XRD patterns of Silicalite-1, Ni-doped zeolites obtained by in-situ synthesis (NS-001, NS-002 and NS-003) and ion-dipped sample Ni-S-1

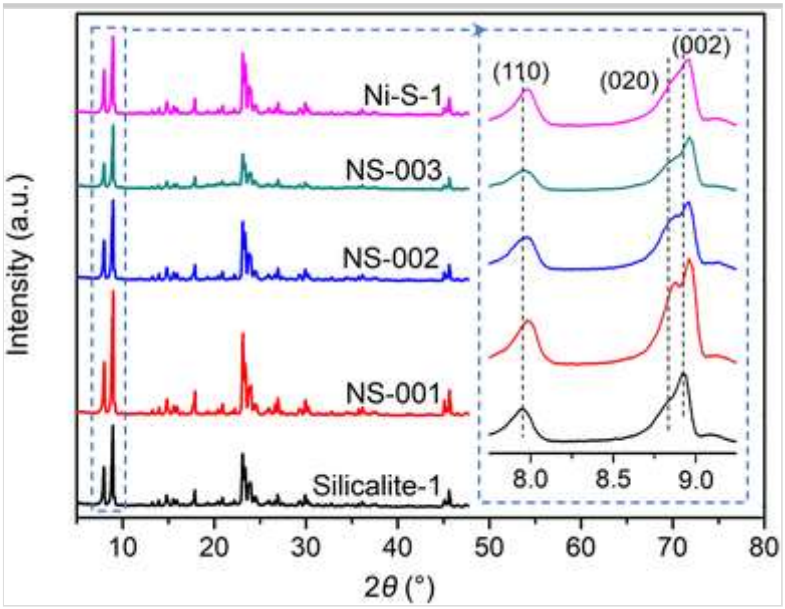

Table 2

Elemental composition in different samples and calculated numbers of Ni atoms per unit cell in the crystals

Catalyst	Mass fraction of Ni content (wt%)	Mass fraction of Si content (wt%)	Number of Ni atoms per unit cell[a]
NS-001	0.81	48.29	0.20
NS-002	1.88	43.62	0.50
NS-003	3.51	42.91	0.90
Ni-S-1	0.36	49.51	0.08

[a]Assuming that there are 24 Si atoms per unit cell

XPS spectra (Fig. 2) have been employed to investigate the interfacial nickel species. The fitted peaks at binding energy around 857 eV in NS-001, NS-002 and NS-003 correspond to Ni^{2+} or Ni^{3+} [30]. In the previous literatures, the surface of nickel oxide can absorb the oxygen molecules under relatively high temperature [31, 32]. Since the samples have been treated at 800 °C, Ni^{2+} should have been translated to Ni_2O_3 even if there was any Ni^{2+} previously. Therefore, we speculate that the peaks originate from the Ni–O bond in Ni_2O_3 [33]. No obvious XPS peaks for nickel species are detected in Ni-S-1 sample, and this can be caused by the nickel element loss at the crystal surface during the preparation process. Considering that XPS can only be used to analyze the surface valence state of a material [34], the introduced nickel species by impregnation could be inside the crystals.

Fig. 2

XPS spectra for **a** NS-001, **b** NS-002, **c** NS-003 and **d** Ni-S-1

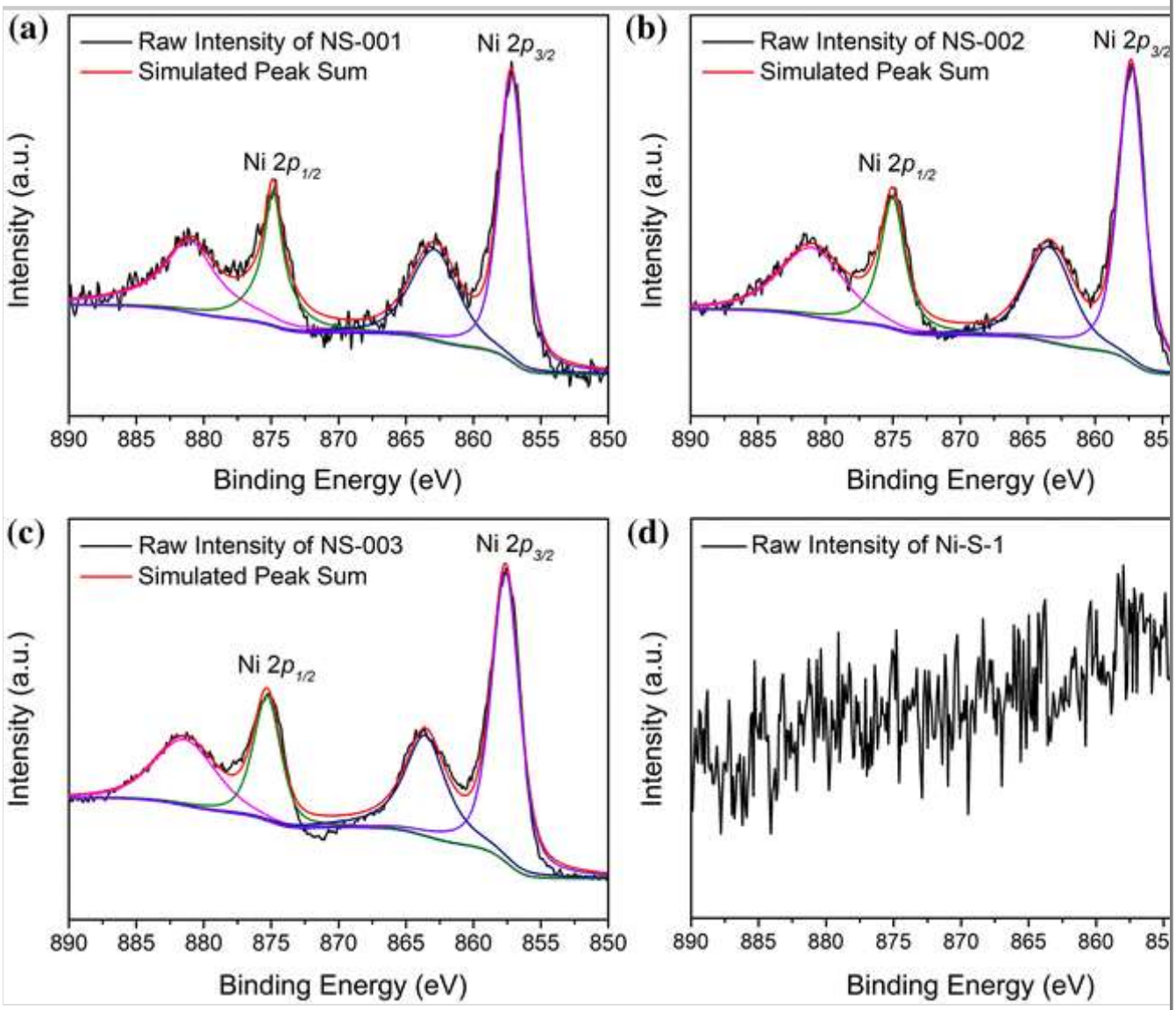

SEM images of the zeolites show the morphology of long rod-like shape with uniform size. No amorphous gel appears in pure Silicalite-1 samples (Fig. 3a). But for the samples of NS-001, NS-002 and NS-003, some amorphous gels appear with the introduction of nickel (Fig. 3b–d). With the amount of nickel contents elevated, more amorphous gels form in the samples. These amorphous gels decrease the zeolite crystallinity, which is consistent with the XRD results. Moreover, the grain size decreases slightly from 20 to 40 μm (Silicalite-1) to 10–30 μm (NS-001, NS-002 and NS-003) due to the depression effect of metal atoms [35, 36].

Fig. 3

SEM images of synthesized samples: **a** Silicalite-1, **b** NS-001, **c** NS-002 and **d** NS-003

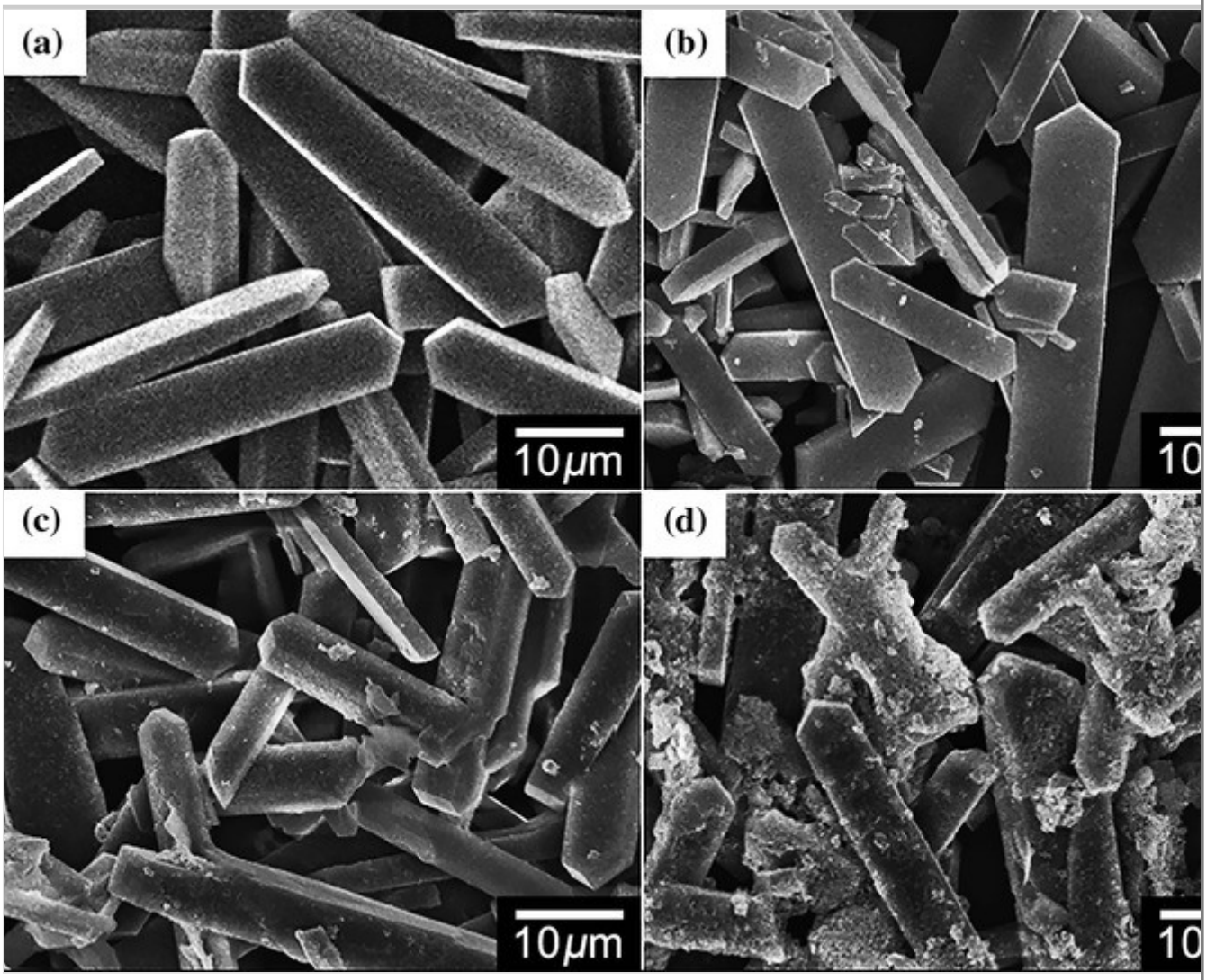

The structural stabilities of the Ni-doped zeolites with different content of nickel are studied by non-isothermal TG and DSC measurements and the results are shown in Fig. 4. As can be seen from TG curves (Fig. 4a), no obvious changes in weight are found for the Ni-doped zeolites under the temperature range from room temperature to 1000 °C. Figure 4b is the non-isothermal DSC curves corresponding to the TG results. No peak is observed beyond 600 °C in the curves of in-situ Ni-doped samples, indicating an excellent structural stability of the zeolites. Therefore, it is demonstrated that introducing nickel by in-situ method has not changed the thermal stability of zeolites. However, the weight of ion-dipped Ni-S-1 increases continuously when the temperature is beyond 400 °C (Fig. 4a), and an obvious endothermal peak is found in the DSC curve (Fig. 4b). We speculate an oxidation reaction ($4\ NiO + O_2 \rightarrow 2\ Ni_2O_3$) [30, 31] may occur once the temperature is above 400 °C, causing the degradation of the thermal stability (Fig. 4b).

Fig. 4

a TG and **b** DSC results of Ni-doped zeolites (NS-001, NS-002 and NS-003) and ion-dipped Ni-S-1

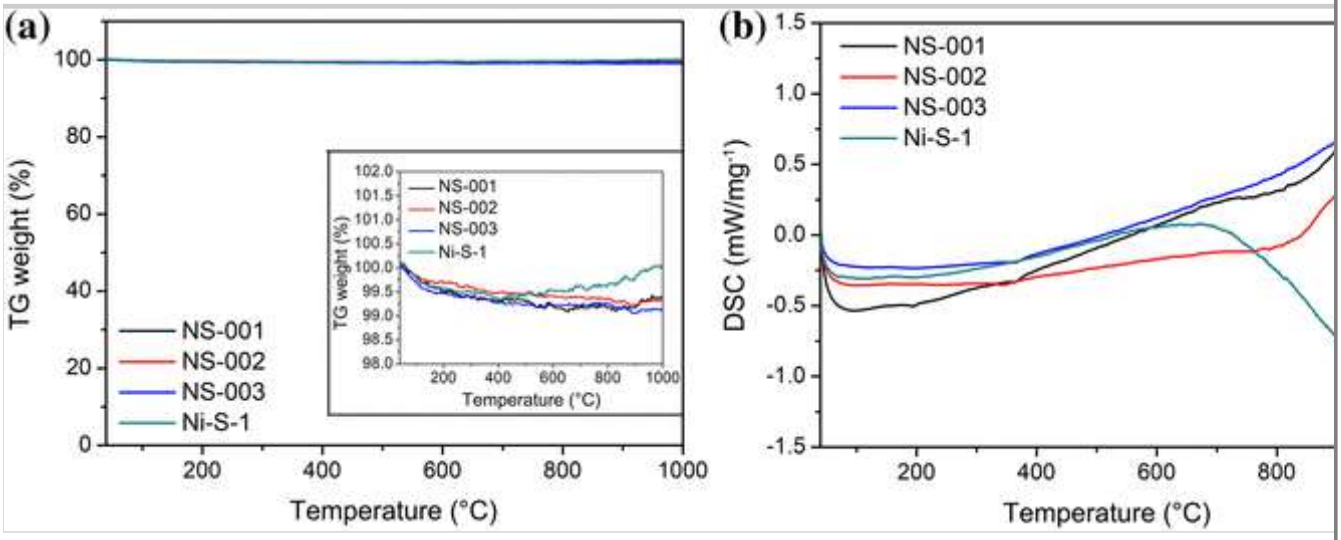

The textural properties (surface area, pore volume and pore diameter) of parent Silicalite-1and the Ni-doped catalysts are listed in Table 3. The pure Silicalite-1 has a BET surface area of 370 m^2/g, a total pore volume of 0.18 cm^3/g, and an average pore size of 20.84 Å. But for Ni-doped Silicalite-1, the surface area and average pore size of NS-001, NS-002 and NS-003 are 332 m^2/g and 26.35 Å, 325 m^2/g and 27.95 Å, 272 m^2/g and 36.70 Å, respectively. It is observed that the BET surface area of the catalysts reduces from 370 to 272 m^2/g, and the average pore size of the catalysts gradually increases from 20.84 to 36.70 Å with the increase of nickel contents, while the total pore volume has slightly decreased. We believe it is attributed to the development of partial strain generated during the incorporation of oxides of nickel [37]. Furthermore, part of NiO_x nanoparticles enter the pores and channels of the zeolites, causing the slightly decrease of total pore volume.

Table 3

Physicochemical properties of pure Silicalite-1 and the in-situ obtained Ni-doped catalysts

Catalyst	S_{BET} $(m^2/g)^a$	V_{total} $(cm^3/g)^b$	d_p $(Å)^c$
Silicalite-1	370	0.18	20.84

Apparent surface area calculated by BET method
Total pore volume at P/P = 0.98
Average pore size calculated BJH method from the N adsorption branch

Catalyst	*S* (m /g)	*V* (cm /g)	*d* (Å)
NS-001	332	0.18	26.35
NS-002	325	0.18	27.95
NS-003	272	0.16	36.70
[a]Apparent surface area calculated by BET method			
[b]Total pore volume at $P/P_0 = 0.98$			
[c]Average pore size calculated BJH method from the N_2 adsorption branch			

The catalytic activity and stability of series of Ni-doped catalysts in dry reforming of COG performed at 800 °C for 36 h are shown in Fig. 5. The conversion of reactants and selectivity of products are calculated and listed in Table 4. For the in-situ doped NS-001, it exhibits the relatively best catalytic behavior with CH_4 and CO_2 conversion of 74.0 and 90.8%, and H_2 and CO selectivity of 72.2 and 92.4%, respectively. But for the traditional ion-dipped Ni-S-1 sample, it is suspected that CH_4 and CO_2 hardly react with each other, resulting in a low CH_4 conversion (2.3%) and a low CO_2 conversion (12.9%). Obviously, the in-situ synthesized Ni-doped catalysts have a much more significant catalytic activity compared with the ion-dipped sample. It can be explained that the uniformly dispersed nickel oxides doped by in-situ method more fully contact with the reactant gases contributing a more complete reaction. Meanwhile, in-situ Ni-doped catalysts demonstrate excellent sustainability during 36 h, indicating they remain stable under relatively high temperature. Among the samples, NS-003 exhibits the relatively inferior catalytic behavior with the CH_4 and CO_2 conversions of 61.2 and 85.0%, which can be caused by its lower crystallinity. The difference between the conversion values of CH_4 and CO_2, as well as the selectivies of H_2 and CO, may result from the secondary reactions occuring in the dry reforming reaction [4].

Fig. 5

Catalytic activity in the dry reforming of COG over Ni-doped Silicalite-1 catalysts. **a** CH_4 conversion, **b** CO_2 conversion, **c** H_2 selectivity, **d** CO selectivity. Reaction conditions: GHSV = 12,000 mL g^{-1} L^{-1}, CH_4/CO_2 molar ratio = 1.0, P = 1 atm, T = 800 °C

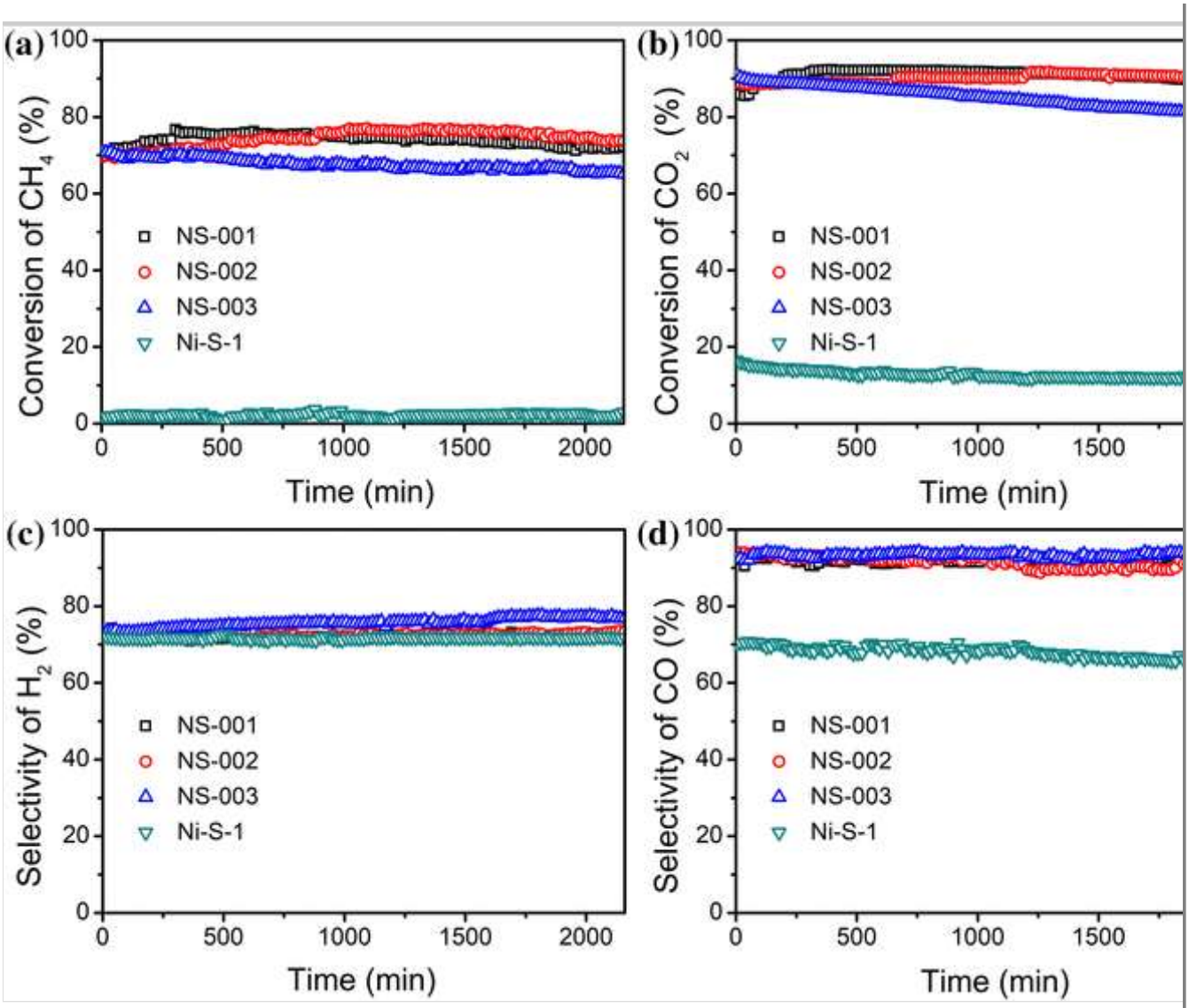

Table 4

Activities of catalytic dry reforming of COG over Ni-doped Silicalite-1 catalysts, and the theoretically calculated turnover frequency (TOF)

Catalyst	Conversion (%)[a]		Selectivity (%)[a]		TOF ($\times 10^6$ h^{-1})	
	CH_4	CO_2	H_2	CO	CH_4	CO_2
NS-001	74.0	90.8	72.2	92.4	1.60	1.96
NS-002	73.7	90.0	72.7	91.4	1.59	1.95
NS-003	61.2	85.0	75.7	96.1	1.32	1.84
Ni-S-1	2.3	12.9	71.7	68.0	–	–
1%-Ni/LZ [b]	84.9	87.8	–	–	0.66	0.68
[a]Experimental values from average results						
[b]TOFs of CH_4 and CO_2 are calculated theoretically according to the data from previous literature [4]						

In order to judge the catalytic performance of the catalysts, we choose the averaged turnover frequency (TOF) during the catalytic process as the evaluation standard. In the field of catalysis, TOF is defined as in unit time, the number of moles of reactants that a mole of active component in a catalyst can convert before becoming inactivated. The reported Ni^{2+}-doped La_2O_3–ZrO_2 material (denoted as 1%-Ni/LZ, the mass fraction of Ni is 0.9%) [38] is also conducted as a contrast. In the literature, Tao et al. investigated 0.5 g 1%-Ni/LZ catalyst's performance for reforming reaction and the corresponding results suggested a remarkable catalytic activity. TOF is calculated based on theoretical data for the in-situ obtained catalysts and Ni/LZ sample (assuming that total mass keeps constant).

$$\mathrm{TOF}_i = \frac{n_{i,\ in} - n_{i,\ out}}{n_{\mathrm{Ni}} \times t} = \frac{P \times F_{i,in} \times X_i}{R \times T \times n_{Ni}} \quad (5)$$

where i means CH_4 or CO_2; $n_{i,in}$ and $n_{i,out}$ represent moles of the inlet and outlet CH_4/CO_2; n_{Ni} means moles of nickel atoms in the catalysts, and the mass fractions of nickel content measured by ICP are listed in Table 2; t means the total reaction time; $F_{i,in}$ means the flow rate of CH_4 or CO_2 in feed gas; X_i means the conversion. The results are illustrated in Table 4.

As shown in Table 4, TOFs of both CH_4 and CO_2 in the reaction catalyzed by in-situ Ni-doped catalysts are more than twice those catalyzed by 1%-Ni/LZ, respectively. It is unquestionable that in-situ prepared catalysts exhibit superior catalytic activity with signally less amount of nickel which is the active component. The highly dispersed nickel species in the crystals which provide more active sites mainly account for the relatively superior TOFs.

XRD patterns of the catalysts after the catalytic reaction are presented in Fig. 6. It shows that the crystal structure of the used catalysts remains during the dry reforming of COG at 800 °C for 36 h. Furthermore, the standard XRD pattern for carbon (the main diffraction at $2\theta = 26.1°$) is not found, revealing a good performance of resistance of carbon deposition of zeolites [39].

Fig. 6

XRD patterns of the in-situ obtained catalysts and Ni-dipped Silicalite-1 after the catalytic reaction

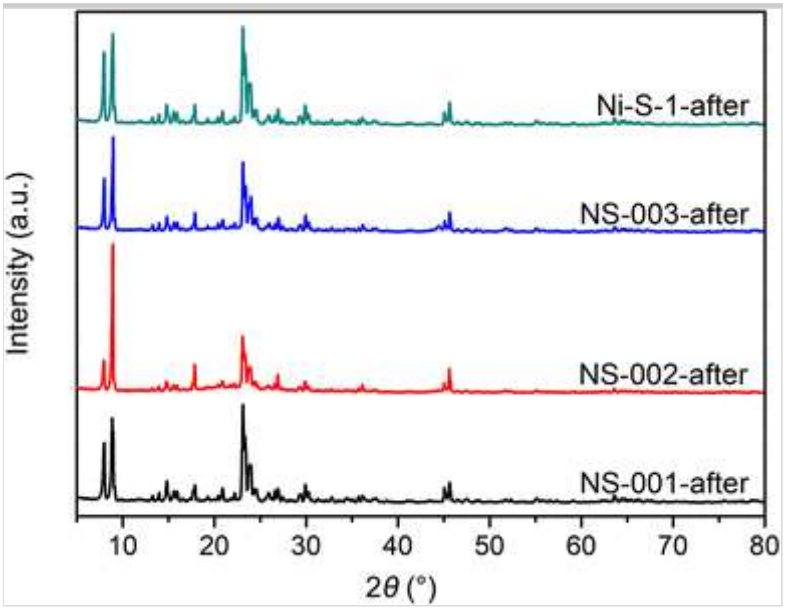

As shown in Fig. 7a, the mass loss from 500 to 650 °C in thermogravimetric curves of used catalysts corresponds to the oxidation of carbon deposited on the catalysts [40]. Compared with a mass loss of lower than 5.0 wt% of the reported Ni/LZ catalysts [38], the slight weightlessness (no more than 0.6 wt%) further indicate a prominent anti-carbon property of the in-situ Ni-doped catalysts. According to the former literature, carbon deposition mainly comes from the pyrolysis of methane and carbon monoxide during the reactions [8]:

Fig. 7

a TG and **b** DSC results of used catalysts after the catalytic reaction

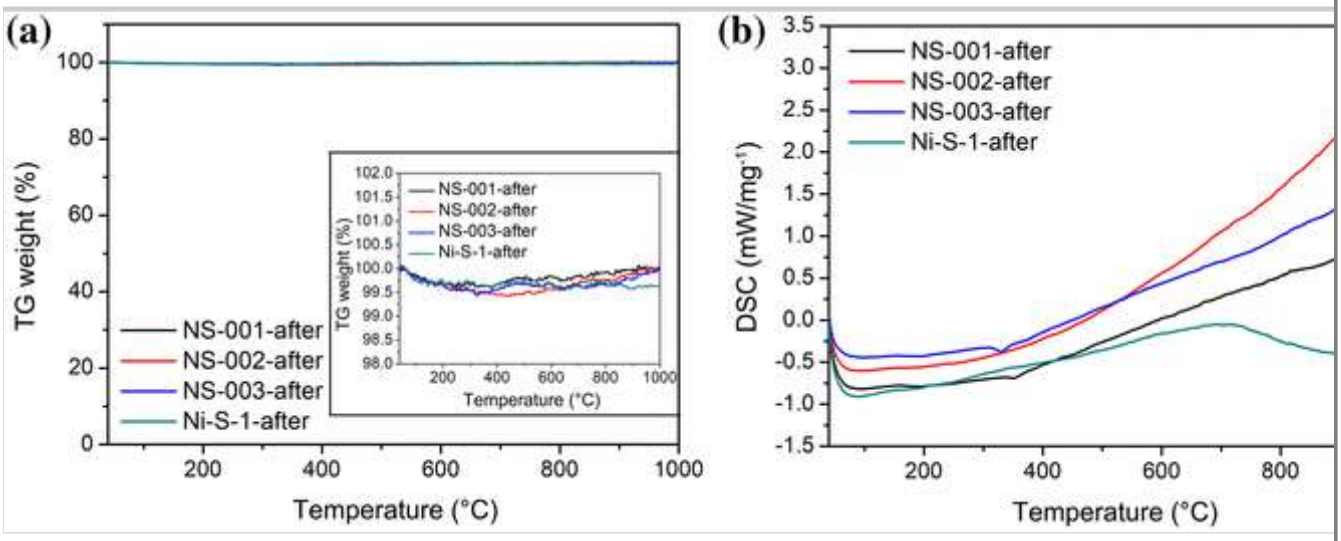

$$CH_4 \rightarrow C + 2\,H_2 \quad (6)$$

$$2\,CO \rightarrow C + CO_2 \quad (7)$$

$$H_2 + CO \rightarrow C + H_2O \quad (8)$$

The superior carbon deposition resistance of in-situ Ni-doped zeolite catalysts is supposed to result from the few occurrences of pyrolysis reactions over the zeolite catalysts. As shown in Fig. 7b, no peak is appeared above 600 °C in the DSC curves of in-situ obtained samples, corresponding to the results of TG.

In order to verify the catalysts' carbon deposition resistance more intuitively, the used catalysts are observed by TEM. As shown in Fig. 8, no obvious carbon deposition is found in the in-situ Ni-doped samples after reaction (Fig. 8b–d), while carbon deposited on the used Ni/LZ catalyst [38] can be easily noticed. Meanwhile, the samples maintain inerratic bar shape without crystallographic defect, further demonstrating the stability of catalysts.

Fig. 8

TEM images of **a** Silicalite-1 and the used Ni-doped catalysts: **b** NS-001, **c** NS-002 and **d** NS-003

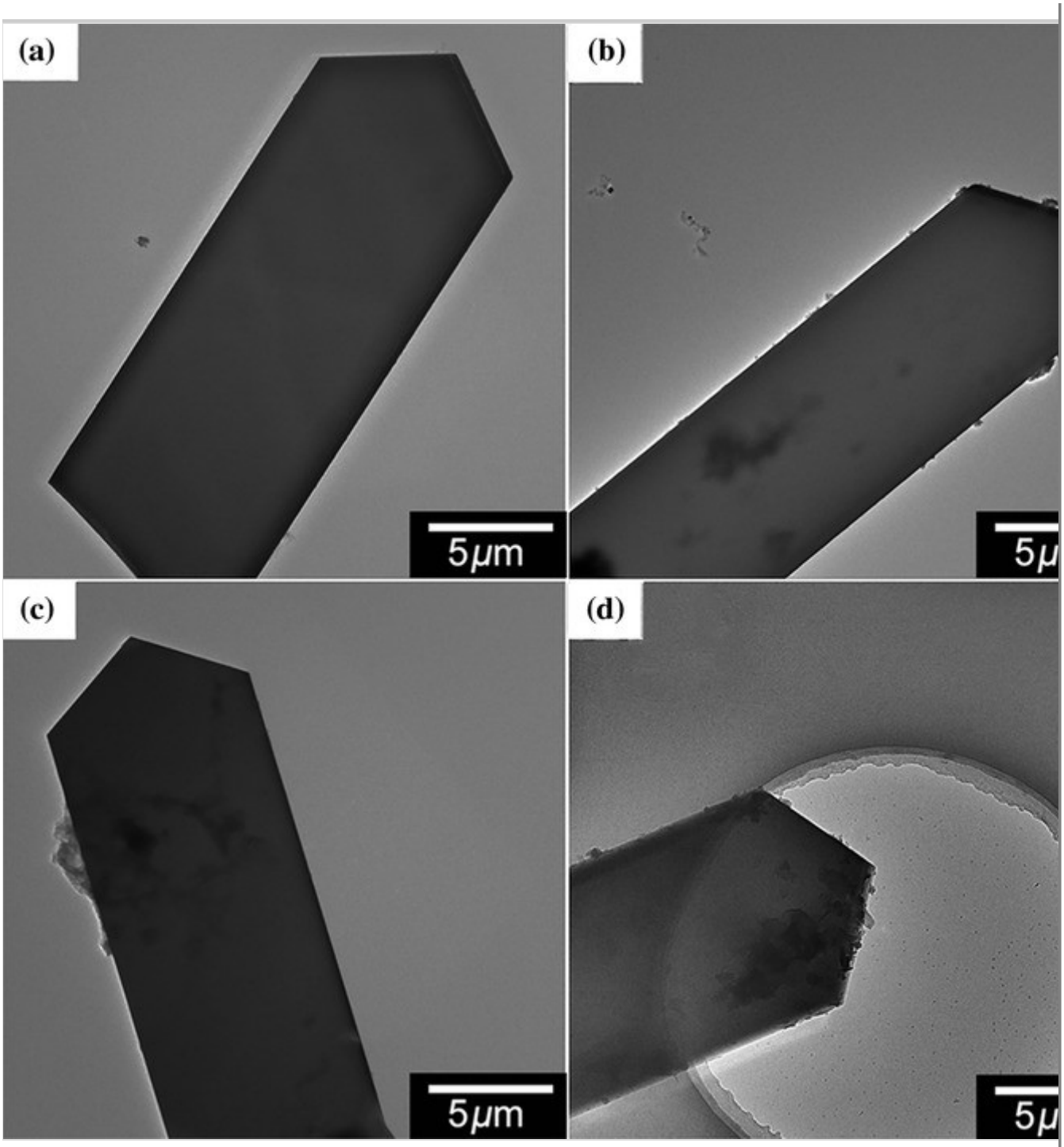

H_2-TPR profiles of the calcined Ni-doped Silicalite-1 catalysts are exhibited (Fig. 9) to investigate the interaction between Ni atoms and the zeolite framework, which could give a further explanation to the catalytic activity of the samples. First of all, we got the ratio of hydrogen consumption (according to the integral area under the peaks): 1.00:3.11:4.87:0.52, corresponding to the ratio of nickel contents in NS-001, NS-002, NS-003 and Ni-S-1 (1.00:2.32:4.33:0.44), respectively. Obviously, there are two broad reduction peaks appeared at 388 and 690 °C (NS-001)/716 °C (NS-002), respectively. With the increase of nickel contents, reduction peaks of NS-003 catalyst shift to the position of 563 and 727 °C, respectively. Ruckenstein and colleagues [41] ever found that reducing ability of the active components over the carrier surface was related to its degree

of aggregation, and highly dispersive active ingredient had a strong interaction with the carrier, resulting in the increase of reduction temperature. Accordingly, the reduction peaks at around 700 °C indicate that nickel species in the in-situ Ni-doped catalysts have a strong reaction with the carrier, resulting in a higher catalytic activity [42]. Simultaneously, reduction peaks with a high intensity and a symmetrical peak shape also manifest that the active nickel species is uniformly distributed in the crystals. Ni species in Ni-S-1 is mainly reduced at low temperature (around 525 °C), and this will cause the migration and aggregation of the introduced nickel [43]. Therefore, the lower Ni dispersion is one of the main reasons why the Ni^{2+}-Silicalite-1 hardly has the catalytic performance.

Fig. 9

H_2-TPR profiles of the calcined catalysts before the catalytic reaction

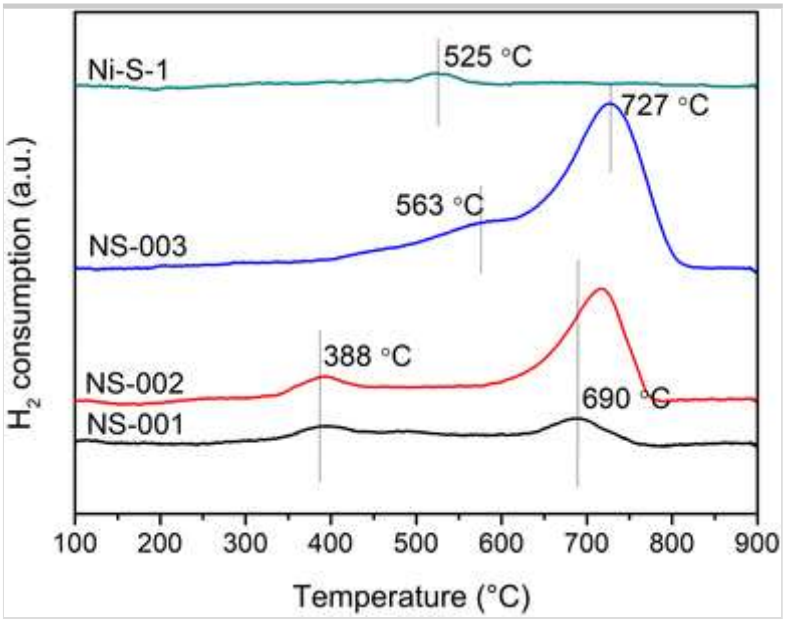

In order to investigate the nature of the carbon deposition, O_2-TPO profiles are conducted for the used catalysts. As shown in Fig. 10, single oxidation peaks are found at lower temperature (vary from 320 to 360 °C), which means only one type of carbon deposition is formed over different Ni-doped catalysts [44]. Furthermore, the deposited carbon possibly be amorphous carbon which is more reactive and could be eliminated by the reactive oxygen species dissociated from CO_2 during the catalytic reaction [45]. Therefore, it is also one reason that carbon deposition is scarcely formed in the in-situ Ni-doped catalysts.

AQ3

Fig. 10

O_2-TPO profiles of the catalysts after the catalytic process

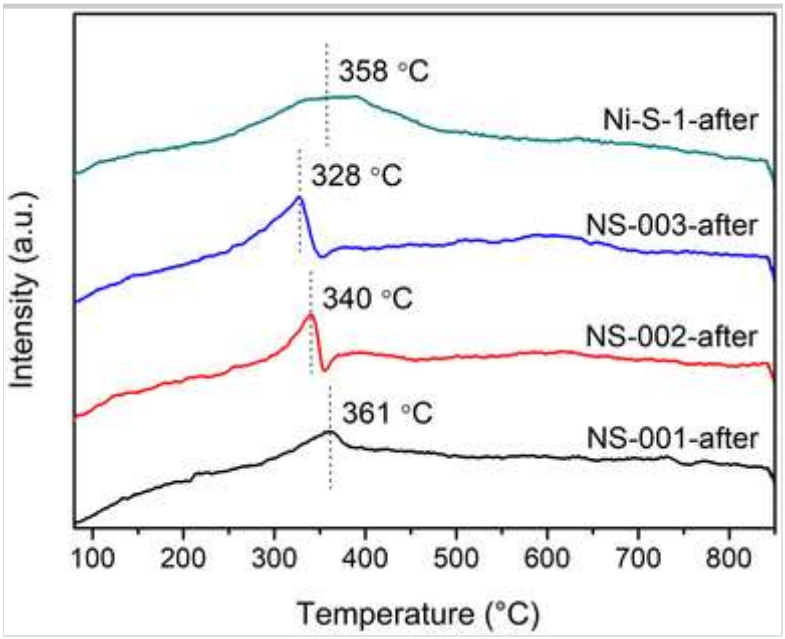

4. Conclusions

Hydrogen production from COG through dry reforming achieved over one-pot hydrothermal synthesized Ni-doped zeolite catalysts are investigated systematically. Highly dispersed nickel element in the crystals is acquired by in-situ preparation process, which gives reactant gases full access to the active sites and contributes to a remarkable catalytic performance. These in-situ Ni-doped zeolites, with high structure stability and strong carbon deposition resistance, have dramatically higher catalytic activity during the dry reforming process than the nickel ion-dipped zeolite. The TOFs of CH_4 and CO_2 can reach 1.60×10^6 h^{-1} and 1.96×10^6 h^{-1}over in-situ Ni-doped Silicalite-1, respectively, which are almost three times those catalyzed by nickel-based La_2O_3–ZrO_2 catalyst. After being evaluated for 36 h under the temperature of 800 °C, the in-situ Ni-doped catalyst can still preserve good structural stability. The novel Ni-doped Silicalite-1 zeolites show a potential application for hydrogen production from COG by dry reforming.

Acknowledgements

This research was supported by National Natural Science Foundation of China (No. 51371112), Shanghai Natural Science Foundation of China (No.17ZR1420000), Shanghai Talent Development Funding for the Project (No.2017077), Innovation Program of Shanghai Municipal Education Commission (No.13ZZ071), and National Key Basic Research Program of China (No. 2014CB643403).

References

1. Christopher K, Dimitrios R (2012) Energy Environ Sci 5:6640–6651

2. Sun T, Zhang C, Chen J, Yan Y, Zakhidov AA, Baughman RH, Xu L (2015) J Mater Chem A 3:11367–11375

3. Dai C, Zhang S, Zhang A, Song C, Shi C, Guo X (2015) J Mater Chem A 3:16461–16468

4. Zhang Y, Li Q, Shen P, Liu Y, Yang Z, Ding W, Lu X (2008) Int J Hydrog Energy 33:3311–3319

5. Wen S, Liang M, Zou J, Wang S, Zhu X, Liu L, Wang Z (2015) J Mater Chem A 3:13299–13307

6. Bermúdez JM, Fidalgo B, Arenillas A, Menéndez JA (2012) Fuel 94:197–203

7. Cheng H, Zhang Y, Lu X, Ding W, Li Q (2009) Energy Fuels 23:414–421

8. Cheng H, Lu X, Zhang Y, Ding W (2009) Energy Fuels 23:3119–3125

9. Rostrup-Nielsen JR, Hansen JB (1993) J Catal 144:38–49

10. Tang S, Ji L, Lin J, Zeng HC, Tan KL, Li K (2000) J Catal 194:424–430

11. Pereñiguez R, Gonzalez-delaCruz VM, Caballero A, Holgado JP (2012) Appl Catal B 123–124:324–332

12. Stagg-Williams SM, Noronha FB, Fendley G, Resasco DE (2000) J Catal 194:240–249

13. Bellido JDA, Assaf EM (2009) Appl Catal A 352:179–187

14. Cheng H, Feng S, Tao W, Lu X, Yao W, Li G, Zhou Z (2014) Int J Hydrog Energ 39:12604–12612

15. Barrera A, Fuentes S, Díaz G, Gómez-Cortés A, Tzompantzi F, Molina JC (2012) Fuel 93:136–141

16. Pompeo F, Nichio N, Ferretti O, Resasco D (2005) Int J Hydrog Energ 30:1399–1405

17. Zhang Z, Li J, Gao W, Ma Y, Qu Y (2015) J Mater Chem A 3:18074–18082

18. Chin Y, King D, Roh H, Wang Y, Heald S (2006) J Catal 244:153–162

19. Guisnet M, Dégé P, Magnoux P (1999) Appl Catal B 20:1–13

20. Chaudhari K, Das T, Rajmohanan P, Lazar K, Sivasanker S, Chandwadkar A (1999) J Catal 183:281–291

21. Hensen EJM, Zhu Q, van Santen RA (2003) J Catal 220:260–264

22. Wang J, Park J-N, Jeong H-C, Choi K-S, Wei X-Y, Hong S-I, Lee CW (2004) Energ Fuel 18:470–476

23. Lempers H, Sheldon R (1998) J Catal 175:62–69

24. Choi M, Na K, Kim J, Sakamoto Y, Terasaki O, Ryoo R (2009) Nature 461:246–249

25. Zhang X, Wang Y, Xin F (2006) Appl Catal A 307:222–230

26. Frontera P, Aloise A, Macario A, Crea F, Antonucci P, Giordano G, Nagy J (2011) Res Chem Intermed 37:267–279

27. Estephane J, Aouad S, Hany S, El Khoury B, Gennequin C, El Zakhem H, El Nakat J, Aboukais A, Aad EA (2015) Int J Hydrog Energy 40:9201–9208

28. Fakeeha AH, Al–Fatesh AS, Abasaeed AE (2012) Adv Mater Res 550–553:325–328

29. Ban T, Mitaku H, Suzuki C, Matsuba J, Ohya Y, Takahashi Y (2005) J Cryst Growth 274:594–602

30. Hoffer B, Dickvanlangeveld A, Janssens J, Bonne R, Lok C, Moulijn J (2000) J Catal 192:432–440

31. Guo J, Liang J, Chu Y, Yin H, Chen Y (2010) Chinese J Catal 31:278–282

32. Deraz NM (2012) Ceram Int 38:747–753

33. Hong ST, Park DR, Yoo S-J, Kim J-D, Park HS (2006) Res Chem Intermed 32:857–870

34. Watts JF, Wolstenholme J (2003) An introduction to surface analysis by XPS and AES. Wiley, Chichester

35. Azam A, Ahmed AS, Ansari MS, Naqvi AH (2010) J Alloy Compd 506:237–242

36. Liu C, Fang L, Zu X, Zhou W (2007) Chinese Phys 16:95–99

37. El-Sheikh SM, Ismail AA, Al-Sharab JF (2013) New J Chem 37:2399–2407

38. Tao W, Cheng H, Yao W, Lu X, Zhu Q, Li G, Zhou Z (2014) Int J Hydrog Energ 39:18650–18658

39. Zheng W-T, Sun K-Q, Liu H-M, Liang Y, Xu B-Q (2012) Int J Hydrog Energ 37:11735–11747

40. Koo KY, Roh H-S, Seo YT, Seo DJ, Yoon WL, Park SB (2008) Appl Catal A 340:183–190

41. Hu YH, Ruckenstein E (2002) Catal Rev 44:423–453

42. Xu J, Zhou W, Wang J, Li Z, Ma J (2009) Chinese J Catal 30:1076–1084

43. Jing Q, Lou H, Mo L, Fei J, Zheng X (2004) J Mol Catal A 212:211–217

44. Noronha FB, Fendley EC, Soares RR, Alvarez WE, Resasco DE (2001) Chem Eng J 82:21–31

45. Rezaei M, Alavi SM, Sahebdelfar S, Yan Z-F (2006) J Nat Gas Chem 15:327–334